Hyperchaotic qualities of the ball motion in a ball milling device

C. Caravati, F. Delogu, G. Cocco, and M. Rustici[a)]
Dipartimento di Chimica, Università di Sassari, Via Vienna 2, I-07100 Sassari, Italy

(Received 1 April 1998; accepted for publication 19 October 1998)

Ball collisions in milling devices are governed by complex dynamics ruled by impredictable impulsive forces. In this paper, nonlinear dynamics techniques are employed to analyze the time series describing the trajectory of a milling ball in an empty container obtained from a numerical model. The attractor underlying the system dynamics was reconstructed by the time delay method. In order to characterize the system dynamics the calculation of the spectrum of Lyapunov exponents was performed. Six Lyapunov exponents, divided into two terns with opposite sign, were obtained. The detection of the positive tern demonstrates the occurrence of the hyperchaotic qualities of the ball motion. A fractal Lyapunov dimension, equal to 5.62, was also obtained confirming the strange features of the attractor. © *1999 American Institute of Physics.* [S1054-1500(99)00101-9]

The synthesis of metastable phases and new materials often requires severe processing conditions. Techniques based on heavy mechanical deformation of solid mixtures have reached a stage of considerable development in the field of materials science. Due to its commercial possibilities and to the unusual physical phenomena involved, powder processing by ball milling still arouses both technological and scientific interest. Energy is transferred from the milling tools to the entrapped powder, which is subject to heavy mechanical loads and undergoes continuous defect accumulation and an ultimate limit of stability is achieved. Diffusion and mass transport phenomena occur through the continuously developed fresh surfaces. The phase transformation and its rate are intimately linked to the energy transfer of the collision event. The efficiency of the transfer depends, in turn, on the degree of elasticity of the collision, which also affects the general features of the milling dynamics. As the elasticity increases, the milling dynamics change from periodic to aperiodic. This behavior can be suitably characterized with the help of nonlinear dynamical analyses. In this paper, a milling system was modeled and the trajectory of a single ball colliding elastically inside the milling container was numerically simulated. Nonlinear dynamics analyses showed that elastic impact conditions determine the occurrence of a hyper-chaotic behavior.

I. INTRODUCTION

Ball milling processes and high energy mechanical treatments (Mechanical Alloying and Mechanical Milling, MA and MM) have became the common method of synthesizing far from equilibrium structures, such as amorphous alloys and nanostructured materials.[1,2] MA processes have branched out into different fields of Material Science. However, fundamental problems in quantifying the MA process still exist.[3,4] Mechanistic aspects of the process and their links with the intensity of the mechanical treatment still have to be clarified. The major difficulty is represented by the complexity of the milling dynamics preventing, for a long time, any accurate measurement of the fundamental milling parameters such as collision frequency and velocity.

A satisfactory, even if partial, solution to the problem was recently accomplished as a result of our efforts. An experimental methodology and a modelistic approach were developed and employed to characterize milling experiments performed with a single milling ball and a variable powder charge. The former is based on the use of a piezoelectric shock sensor to detect the ball–vial collisions coupled with a magnetic vial position survey system to locate the vial at the impact instants, whilst the latter is based on numerical techniques.[5,6]

Due to the cushioning effect of the powder entrapped between the ball and the container, the powder amount strongly affected the elasticity degree of the ball–vial collisions. Therefore, depending on the powder load, the milling regime progressively changed from plastic to elastic, and we attempted to simulate it by using a restitution coefficient changing, respectively, from 0 to 1.

At a low elasticity degree, impacts were observed to occur with a high periodicity, allowing for an accurate experimental evaluation of the frequency and the velocity of the collisions. A regular and periodic ball trajectory also resulted from the numerical simulation. The experimental approach and the numerical calculations sustained each other. Full details are reported elsewhere.[6]

Besides the valuable support to the experimental methodology, the modeling approach offered a deeper insight into the milling dynamics, allowing one to extend the investigation from plastic to elastic impact conditions. Indeed, by decreasing the powder charge, the ball motion gradually lost its regularity, the impact frequency increased, and, finally, at the highest degrees of elasticity, the motion became aperiodic. In these conditions the milling parameters, mostly the impact velocity, were no longer experimentally measurable. Under these circumstances, numerical calculations supplied a ball trajectory of high complexity.

a)Corresponding author; electronic mail: rustici@ssmain.uniss.it

The ball trajectory can be regarded as a complex time series characterized by apparent randomness. In the present paper, the time series was analyzed by nonlinear dynamics techniques in order to point out the occurrence of chaotic behavior and to better characterize the link between periodicity loss and impact quality.

''Chaos'' and ''chaotic'' are distinguishing terms used to describe the aperiodic and apparently random time behavior of a deterministic system with a small number of degrees of freedom.[7,8] The time evolution of a deterministic physical system is often described according to a set of ordinary differential equations (ODE),

$$\frac{d\mathbf{u}(t)}{dt}=\mathbf{F}(\mathbf{u}(t),\mu), \tag{1}$$

where t is the elapsed time and μ are one or more parameters on which the system behavior depends. The n-dimensional space of the state vectors $\mathbf{u}(t)=(u_1(t),u_2(t),\ldots,u_n(t))$ is called phase space. In this space, the time evolution $\mathbf{u}(t)$ describes the trajectory or orbit of motion. Depending on the linearity or nonlinearity of the vector field $\mathbf{F}(\mathbf{u})$, the system is said to be linear or nonlinear. The mathemathical complexity of nonlinear systems can be partially overcome by resorting to the study of the qualitative aspects of the dynamics, corresponding to the topological properties of the phase space trajectory $\mathbf{u}(t)$ as $t\to\infty$. In the case of dissipative systems the orbit $\mathbf{u}(t)$ asymptotically converges to a subset of the phase space with its own geometry and dimension, strictly less than the phase space one. Such a subset is called the attractor of the system.

In the case of a chaotic system, the attractor has very complex geometric features mirroring the apparently random time evolution. Often a noninteger attractor dimension results. A similar fractal object is referred to as a strange attractor.

The fundamental property of a chaotic dynamical system is its sensitivity to the initial conditions. Small differences in the initial conditions lead to an exponential divergence of the related trajectories in the phase space. A formal account of this property can be obtained by introducing the Lyapunov exponents.[8] These express the average rates with which the trajectories exponentially diverge or converge along each of the n directions in the phase space. Any system possessing at least one positive Lyapunov exponent is defined as chaotic. If more than a single positive Lyapunov exponent is found, the system is defined as hyperchaotic.

Together with Lyapunov exponents, fractal dimensions, which characterize the distribution of the attractor points in the phase space, have emerged as useful classifiers of chaotic motion.[9–11]

Nonlinear dynamics analysis techniques are suitable for the problem at hand.

II. RESULTS AND DISCUSSION

A. The model

We refer to a Spex Mixer/Mill mod. 8000. An electrical engine communicates the motion to a mechanical arm mounted in an eccentric fulcrum. The mechanical arm swings a cylindrical container, 5.8 cm high and 3.8 cm in diameter, along a three-dimensional course with a frequency variable between 14.6 and 22.5 Hz. The main component of the vial motion is an angular harmonic displacement on the vertical plane coupled with a sincronous rotation on the equatorial plane. A sketch of the vial motion is shown in Fig. 1.

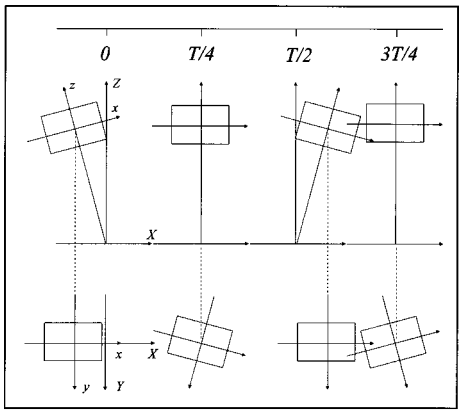

FIG. 1. Typical course of the Spex Mill. The vial motion is shown on the vertical $(X;Z)$ and on the equatorial $(X;Y)$ planes. The main component is a harmonic swing occurring over a shallow arc on the vertical plane. As shown in the lower graph, a synchronous additional movement makes the vial rotate around its barycenter on the $(X;Y)$ plane.

The model starts with the analytical description of the vial motion. With reference to this, the dynamics of the system vial–ball was reproduced by a computer simulation. The frequency of the vial motion was $\nu=18.3$ Hz. A single ball, having a diameter of 1.24 cm, was considered.

1. The analytical equations of the vial motion

The vial motion can be described as a combination of synchronous rototranslations with reference to a fixed frame of Cartesian axes.

Two Cartesian reference systems are considered: an inertial one, of co-ordinates $(X;Y;Z)$, centered on the fulcrum of the mechanical arm, and a second, noninertial one of coordinates $(x;y;z)$, moving with the vial and with the origin coincident with its baricenter. The two reference systems are shown in Fig. 2. The continuous and periodic angular displacement of the mechanical arm (that is, of the distance vector R) is described by the following equation:

$$\theta=\theta_0\cos(\omega t+\delta), \tag{2}$$

where θ_0 is the amplitude of the angular motion, $\omega=2\pi\nu$ and ν is the frequency of the motion. δ is a phase factor dependent on the initial conditions. The oscillation of the mechanical arm around its own axis of an angle α, generating the oscillation of the vial in the $(X;Y)$ plane, is ruled by an analogous equation:

$$\alpha=\alpha_0\sin(\omega t+\delta). \tag{3}$$

The angles θ and α have a phase difference equal to $\pi/2$. θ_0 and α_0 correspond to 15°, while R is equal to 10 cm.

The following sets of equations:

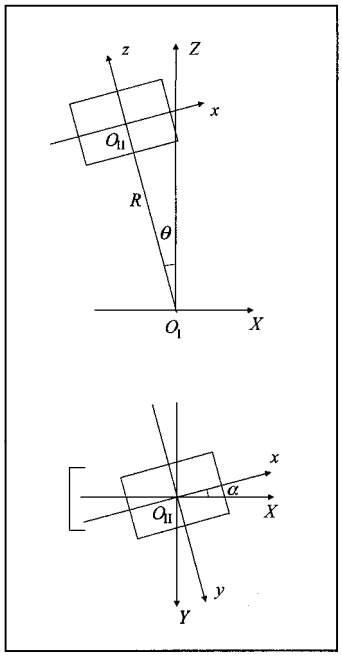

FIG. 2. Inertial $(X;Y;Z)$ and noninertial $(x;y;z)$ reference frames used to represent the vial motion. The vial, centered at the origin O_{II} of the latter, is also depicted. It oscillates on both the $(X;Z)$ and $(X;Y)$ planes with a $\pi/2$ phase difference. R represents the distance between the points O_I and O_{II}, corresponding to the origins of the two reference frames.

$$X=(x\cos\alpha+y\sin\alpha)\cos\theta+(z+R)\sin\theta,$$
$$Y=-x\sin\alpha+y\cos\alpha, \tag{4}$$
$$Z=-(x\cos\alpha+\sin\alpha)\sin\theta+(z+R)\cos\theta,$$

and

$$x=(X\cos\theta-Z\sin\theta)\cos\alpha-Y\sin\alpha,$$
$$y=(X\cos\theta-Z\sin\theta)\sin\alpha+Y\cos\alpha, \tag{5}$$
$$z=X\sin\theta+Z\cos\theta-R,$$

describe the displacement of a point with co-ordinates $(x;y;z)$ and $(X;Y;Z)$, in the noninertial and inertial reference systems, as a function of the time. Consequently, the motion of any point of the vial is analytically known. Given a point of co-ordinates $(x;y;z)$ belonging to the vial, it is possible to follow its three-dimensional trajectory by applying the equations set (4). The inertial co-ordinates of the center of a vial basis during a whole vial cycle are compared to the experimental ones in Fig. 3.

The components of the velocity can be obtained by performing a simple time derivative of the previous sets of equations. A further derivation gives the components of the acceleration. Both the velocity and acceleration components values are quoted in Fig. 4.

2. The reconstruction of the ball motion

The ball motion is governed by the impulsive forces acting during each collision, and no analytical expression for the complete ball trajectory can be obtained. However, the ball displacement as a function of the time can be followed step-by-step by numerical modeling. The time step δt was

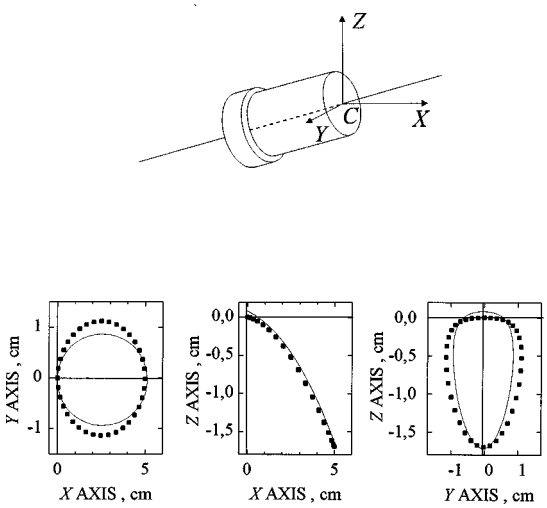

FIG. 3. The upper diagram shows the vial and the center, C, of the vial base. The dots in the diagram below are the experimentally determined co-ordinates of C on the three planes during a complete cycle. The continuous line shows the displacement of C as calculated by the model. Notice the different scale in the axes of the three diagrams. The difference in the maximum displacement along the Y axis arises because the model does not take into consideration the effects of the retaining spring of the clamp assembly.

set equal to 10^{-5} s, in order to have a collision duration equal to the time step and roughly in agreement with data obtained from the Hertzian theory of impact.[12,13]

The ball motion will be uniform rectilinear if external forces are absent. This is always the case, except for the impact events. Between two following collisions, the course of the ball was described by the following Taylor algorithms:

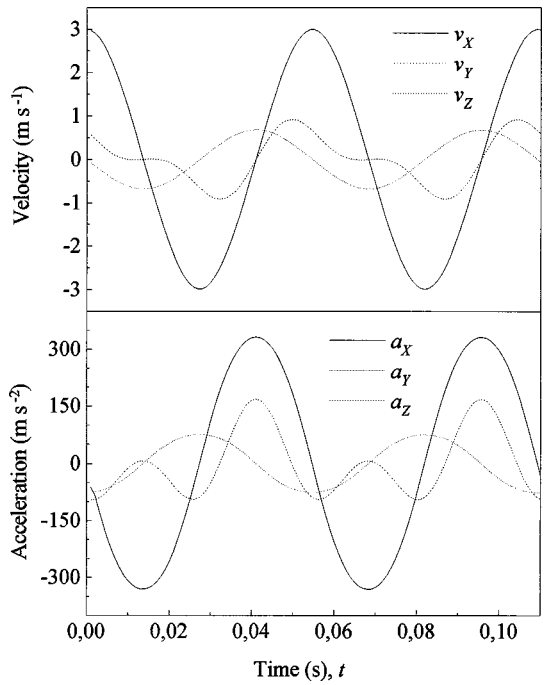

FIG. 4. Velocity (upper pattern) and acceleration (lower pattern) components, on the three orthogonal axes, of the vial motion, obtained from the model. Continuous, dotted and broken lines refer to the X, Y and Z components, respectively.

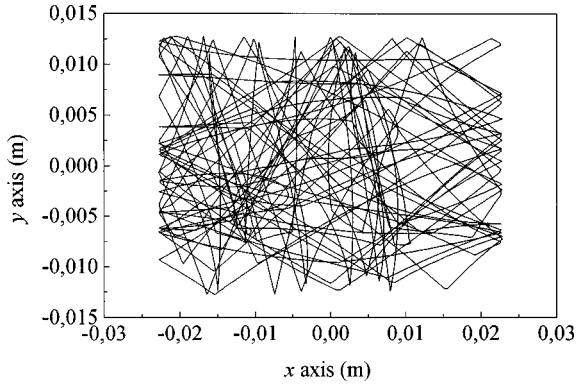

FIG. 5. Projection of a 1 s ball course on the $(x;y)$ plane. For a 1.24 cm diameter ball, the vial has an effective length of 4.56 cm. Therefore collisions at the opposite vial bases occur at $x=2.28$ cm and $x=-2.28$ cm.

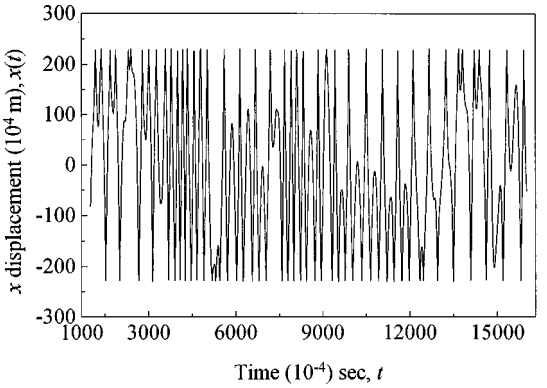

FIG. 6. The ball displacement along the noninertial x axis. Inversions at the maximum displacement points correspond to collisions occurring on the vial bases. The other trajectory inversions and irregularities are due to rebounds on the cylindrical side.

$$X_b(t+\delta t)=X_b(t)+v_{X_b}(t)\ \delta t,$$
$$Y_b(t+\delta t)=Y_b(t)+v_{Y_b}(t)\ \delta t, \tag{6}$$
$$Z_b(t+\delta t)=Z_b(t)+v_{Z_b}(t)\ \delta t,$$

where $X_b(t)$, $Y_b(t)$ and $Z_b(t)$ are the ball center co-ordinates and $v_{X_b}(t)$, $v_{Y_b}(t)$ and $v_{Z_b}(t)$ are the components of the velocity in the inertial reference system. The noninertial ball center co-ordinates $(x_b;y_b;z_b)$ were confined inside a region of space corresponding to the effective volume available for the ball inside the vial. Therefore, the geometrical constraints to the ball motion, which determine the impact conditions, are the following:

$$-2.28<x_b<2.28 \quad \text{cm}, \quad (y_b^2+z_b^2)^{1/2}<1.28 \quad \text{cm}. \tag{7}$$

At each step, the inertial reference frame $(X_b(t);Y_b(t);Z_b(t))$ co-ordinates of the ball were updated. From that, the noninertial reference frame $(x_b(t);y_b(t);z_b(t))$ ball co-ordinates were calculated. The collisions were considered as completely elastic and, at each impact, the velocity vector was modified: the component of the noninertial reference system velocity perpendicular to the surface of impact was simply reversed.

In Fig. 5 a ball trajectory 1 s long was projected on the $(x;y)$ plane. It is possible to appreciate the disordered motion of the ball together with the inversion points of its traveling due to the collisions with the container walls. As evident from Fig. 4, the acceleration experienced by the ball was generally one order of magnitude greater than the gravity and this, together with the shortness of the ball mean free path, enabled us to consider the gravity acceleration as negligible when compared to the acceleration imparted by the vial.

B. Data analysis

A time series of 5.1×10^5 co-ordinates was generated by the numerical solution of equations of motion, corresponding to a ball trajectory of 5.1 s. A data set consisting of six variables was created; the ball co-ordinates $(x(t),y(t),z(t))$ and the velocities $(\dot{x}(t),\dot{y}(t),\dot{z}(t))$ were obtained. To simplify the notation, the lowerscripts (b) were disregarded. According to the embedding theorem and the delay vector method,[8,10] which will be described later on in the paper, any component or scalar function of the state vector can be used to obtain information on the geometry of the attractor. On this basis, the ball displacement along the vial axis, i.e., the $x(t)$ variable, was chosen in order to characterize the ball motion.

The data set was downsampled by a factor of 10 resulting in an effective sampling period of 10^{-4} s. Although the sampling period is 10 times longer than the time step used to numerically solve the equations of motion, it allows a good reproduction of the features of the ball trajectory. The initial transient of 1000 data was skipped to let the system settle down on the attractor and reach the stationary state. As a result, the analysis was performed on a data set consisting of 5×10^4 points. A sketch of the trajectory $x(t)$ is shown in Fig. 6 as a function of the time t. With reference to the vial axis, the absolute maxima and minima in the plot indicate the occurrence of impacts between the ball and the vial bases. Asymmetries and secondary maxima and minima can reasonably be attributed to head-on impacts and near-collisions taking place on the vial cylindrical wall.

1. Power spectrum

The amplitude and power spectra of the time series were calculated on $2^{15}=32768$ data. A Fast Fourier Transform (FFT) algorithm was used. The data are shown in Fig. 7. The amplitude spectrum presented in Fig. 7(a) shows a distribution of discrete frequencies superimposed on a broad continuous band. The most intense peak at 18.3 Hz corresponds to the experimental frequency of the vial course.

Features in the range between 33.5 and 45 Hz emerges, but any detailed assignment is prevented by the complexity of the system dynamics. The power spectrum, quoted in Fig. 7(b), exhibits a slow featureless decay. However, both stochastic and chaotic systems could display such Fourier spectra, and then no evidence can be drawn about the occurrence of chaotic behavior. To characterize such a behavior, further investigation in the appropriate phase space is necessary.

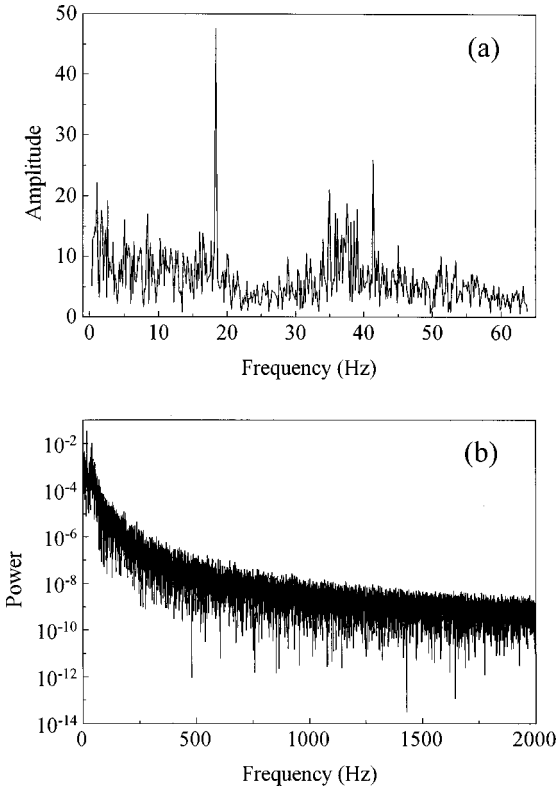

FIG. 7. Amplitude (a) and power (b) spectra as obtained by FFT analyses on the time series.

2. Attractor reconstruction

As previously mentioned, the attractor will be reconstructed by applying the delay vector method. Let us consider the data set as $\{x_i\}=x(t=t_0+i\,T_S)$ where $i=1,2,\ldots,N$, $N=50000$ being the number of samples and $T_S=10^{-4}$ s the sampling period. According to the delay vector method, the trajectory in an m-dimensional phase space is reconstructed by the consecutive m-dimensional vectors,

$$\begin{aligned}
&\mathbf{y}_1=(x_1,x_{1+T},x_{1+2T},\ldots,x_{1+(m-1)T}),\\
&\mathbf{y}_2=(x_2,x_{2+T},x_{2+2T},\ldots,x_{2+(m-1)T}),\\
&\quad\vdots\\
&\mathbf{y}_r=(x_r,x_{r+T},x_{r+2T},\ldots,x_{r+(m-1)T}),
\end{aligned}\tag{8}$$

where m is an integer number called embedding dimension and T is some integer multiple of the sampling period T_S called time delay. The number of reconstructed vectors r is chosen in order to satisfy $r+(m-1)T\leqslant N$. Thus the dynamics is said to be embedded in a m-dimensional phase space. The underlying assumption is that the geometry and the dynamics of the trajectory obtained in this way are the same as the geometry and dynamics of the trajectory in the actual phase space of the system. In particular, the invariants of the system dynamics are the same.[8–11,14] This assumption is verified when a proper choice of the time delay and of the embedding dimension is made.[15]

The time delay T should be large enough to make the consecutive components x_j and x_{j+T} of the reconstructed vectors $\{\mathbf{y}_i\}$ independent. However, the time delay should be not so large as to prevent the statistical independence of x_j and x_{j+T} and the consequent complete uncorrelation of the vectors $\{\mathbf{y}_i\}$. On the contrary, when T is too small, the embedding vectors will cluster in the embedding space around a 45° line passing through the origin, because of the nearly same numerical values of all the components.

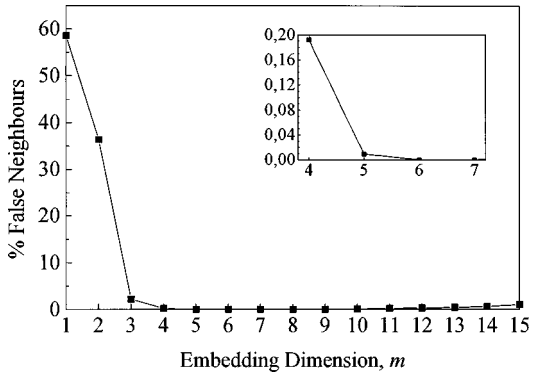

FIG. 8. The percentage of false neighbors using $T=23$ as determined by the average mutual information. As evident from the inset, the percentage drops to zero at $m=6$ which can be identified as the real embedding dimension m_E.

According to Fraser and Swinney,[16] the time delay was chosen in correspondence to the first minimum of the average mutual information function $I(T)$, which is a kind of nonlinear correlation function of the data set $\{x_i\}$. A time delay $T=23$ was obtained.

All the numerical calculations were performed using the cspW package.[17]

The choice of the embedding dimension m is also critical to get a good reconstruction. The uniqueness theorem about the solutions of autonomous differential equations guarantees that no overlap of the orbit with itself is possible in the original phase space.[8] The same must be required to the reconstructed trajectory in the embedding space. The smallest m value allowing for the unfolding of the reconstructed trajectory identifies the proper embedding dimension m_E. If m is smaller than m_E, orbit overlapping occurs due to the projection of the trajectory in a space with a too low dimension. Then, points move closer in the embedding space and become false neighbors. Two nearest neighbors (NN) $\mathbf{y}_i$ and $\mathbf{y}_i^{NN}$ are false nearest neighbors if they are nearest neighbors in dimension m but not in dimension $m+1$. Therefore it becomes possible to identify the proper embedding dimension m_E by calculating the percentage of false nearest neighbors increasing step by step the embedding dimension m.[18] Moving from m to $m+1$ will sequentially remove folding effects and the corresponding percentage of false neighbors will decrease. When the number of false neighbors drops to zero, the attractor is unfolded and remains unfolded in higher dimensions. Consequently, the proper embedding dimension m_E is identified as the embedding dimension for which the percentage of false nearest neighbors drops to zero.

In Fig. 8 the percentage of false neighbors versus increasing values of m is reported. The inset points out a proper embedding dimension $m_E=6$.

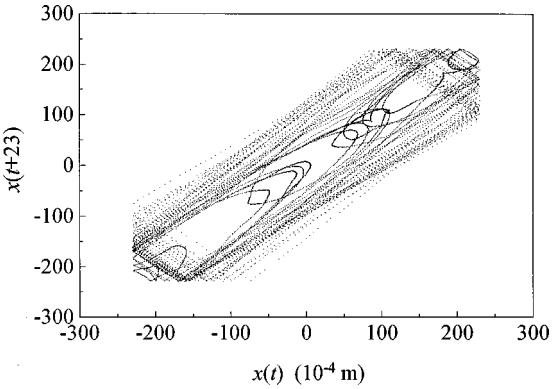

FIG. 9. Projection of the reconstructed attractor on the plane (x_i, x_{i+T}), with a time delay of $T=23$, is shown.

A bidimensional projection of the reconstructed attractor on the plane $(x(t), x(t+23))$ is shown in Fig. 9.

3. Spectrum of Lyapunov exponents

In order to draw a conclusion about the chaotic nature of the dynamics it is necessary to calculate the spectrum of Lyapunov exponents (SLE). A brief outline of the procedure is given below.

Consider a system of n degrees of freedom for which the evolution equation (1) is known. Next, consider the points inside a hypersphere of initial states centered on some point $\mathbf{u}_0$ on the attractor. Let $\epsilon(\mathbf{u}_0)$ be the sphere radius. In general, as time goes on, the flux $\mathbf{F}$ stretches the sphere in one or more directions, contracting it in others. As a result, at the time t the sphere will be distorted in a hyperellipsoid (whose volume will contract to zero for a dissipative system) with n principal axes $\epsilon_k(t)$,

$$\epsilon_k(t) \simeq \epsilon(\mathbf{u}_0)\, e^{\lambda_k(\mathbf{u}_0)\, t}, \quad k=1,2,\ldots,n. \tag{9}$$

The n local Lyapunov exponents are then obtained as

$$\lambda_k(\mathbf{u}_0) = \lim_{t\to\infty} \lim_{\epsilon(\mathbf{u}_0)\to 0} \frac{1}{t} \ln \frac{\epsilon_k(t)}{\epsilon(\mathbf{u}_0)}, \quad k=1,2,\ldots,n, \tag{10}$$

where the notation emphasizes the $\lambda_k(\mathbf{u}_0)$'s dependence on the initial state $\mathbf{u}_0$. The average Lyapunov exponents are obtained by averaging over all the points $\mathbf{u}_0$ belonging to the trajectory. The resulting Lyapunov exponents set $(\lambda_1 \geqslant \lambda_2 \geqslant \ldots \geqslant \lambda_n)$, is referred to as the spectrum of Lyapunov exponents. For an n degrees of freedom system there are n Lyapunov exponents, each one reflecting the orbital stability along a proper direction. The system behavior will become more chaotic at increasing the number of positive Lyapunov exponents. The largest one, λ_1, is the main one responsible for determining the chaoticity of motion. Its value directly reflects the degree of chaos and then the timescale on which its dynamics becomes impredictable.

The SLE calculation needs to know how the sphere is distorted and hence to know the flux $\mathbf{F}$. However, when only the time series of one dynamical variable is known, the flux is obviously unknown. Even if the attractor is made available by the reconstruction method, no information about the underlying dynamics is available—actually the dynamical operator $\mathbf{f}$, mapping the reconstructed attractors $\mathbf{y}_{n+1}=\mathbf{f}(\mathbf{y}_n)$, is unknown. The various methods proposed to evaluate the Lyapunov exponents[9,19–24] mainly differ from one another in the way to cope with this problem. However, all of them consider the trajectory defined by the reconstructed attractor (8) as a fiducial trajectory. The information necessary to the SLE calculation is extracted by following the behavior of nearby trajectories (trajectories arising from points nearby the fiducial trajectory which are considered as initial conditions). In order to reach this goal, in the neighborhood of the fiducial trajectory an approximate reconstruction of the unknown dynamics $\mathbf{f}$ has to be performed.

In the present paper, the Brown *et al.* algorithm[10,24,25] was used. It approximates the dynamics $\mathbf{f}$ by polynomials of degrees p, with $p>1$.

An additional problem is related to the unknown number of degrees of freedom (corresponding to the number of Lyapunov exponents). In fact, the embedding dimension m_E of the reconstructed attractor will be, in general, larger than or equal to the unknown number of degrees of freedom d_L. This arises because of the nonlinear relationships linking the real trajectory $\mathbf{u}(t)$ and the reconstructed one $\{\mathbf{y}_i\}$. Consequently, a working procedure is needed to obtain d_L from the time series. Subsequently it will be possible to calculate the values of the d_L Lyapunov exponents.

The method used to calculate the number of dynamical degrees of freedom, d_L, is based on the evaluation of the percentage of local false nearest neighbors.[25] It explores the local structure of the phase space to check if a local dimension less than m_E is able to capture the evolution of the orbits as they move on the attractor. Consider the attractor reconstructed in a working space with dimension $d_W \geqslant m_E$ to guarantee its complete unfolding. Chosing a point $\mathbf{y}_i$ on it, define a neighborhood by specifying the number of neighbors N_B of the point $\mathbf{y}_i$. The evolution of the N_B points after a time step is provided by a local polynomial map in a d_L-dimensional subspace of the d_W-dimensional space. The dimension d_L is sequentially increased until the percentage of bad predictions becomes independent from d_L and insensitive to neighbors number N_B. This condition identifies the proper d_L dimension.

The percentage of bad predictions versus the local dimension for different values of neighbors N_B is plotted in Fig. 10. A local dimension of $d_L=6$ is clearly identified by the convergence of the different curves. It can be noticed that the coincidence between the d_L value and the m_E is fortuitous, while the correspondence with the degrees of freedom of the system indicates that all of them active. The same results are obtained by evaluating the local false neighbors reading the data backward in time, confirming $d_L=6$ as the local dimension.

It is now possible to calculate the values of the six Lyapunov exponents.[10,24,25] For each pair of initial locations, one of them being on the fiducial trajectory, the behavior of two nearby trajectories is followed for Γ steps of the sampling time forward. The average Lyapunov exponents were obtained by averaging over 5000 initial locations.

In Fig. 11 the plot of the average local Lyapunov exponents λ_k versus the number of steps Γ forward from each

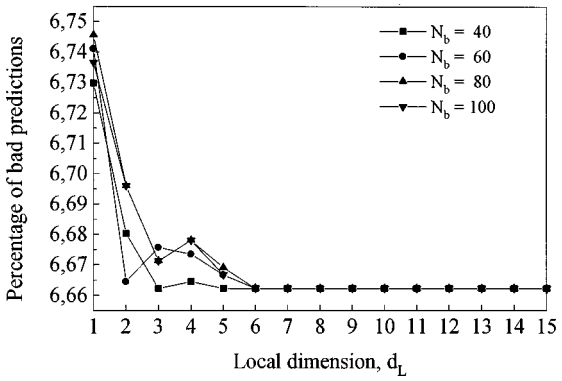

FIG. 10. The percentage of bad predictions as a function of local dimension d_L and number of neighbors N_B. The previously determined $T=23$ was used. The curves converge at $d_L=6$. A same result is obtained if the local false neighbors are evaluated by examining the data backwards in time.

initial location on the attractor is shown. From the spectrum of Lyapunov exponents at $\Gamma=1024$ it results that $\lambda_1=0.49\pm0.05$, $\lambda_2=0.29\pm0.05$, $\lambda_3=0.15\pm0.04$, $\lambda_4=-0.02\pm0.007$, $\lambda_5=-0.31\pm0.01$, $\lambda_6=-0.97\pm0.03$, in inverse units of $T_S=10^{-4}$ s. By carrying out the calculation backward in time, the same results were obtained with a reverse sign. Thus, the Lyapunov exponents divide into terns of values with opposite sign. According to the conventional notation, the spectral signature is $(+,+,+,-,-,-)$. The occurrence of three Lyapunov exponents allows us to claim the hyperchaotic nature of the system under examination. Moreover, as expected in the case of a dissipative system,[7,8] the sum of the Lyapunov exponents $\Sigma_{k=1}^{6}\lambda_k=-0.37\pm0.18$ is negative. It is possible to observe that no zero Lyapunov exponent was obtained. The last observation confirms that the dynamics of the system vial-ball can not be generated by a continuous flow, i.e., by a set of differential equations.[8,10]

4. Lyapunov dimension

There is a close relationship between the Lyapunov spectrum of a chaotic attractor and its fractal dimension. Kaplan and Yorke[8,26] suggested that the spectrum of Lyapunov exponents can be used to evaluate the fractal dimension. They defined

$$D_L=j+\frac{\Sigma_{k=1}^{j}\lambda_k}{|\lambda_{j+1}|}, \tag{11}$$

where D_L is called the Lyapunov dimension (or Kaplan Yorke dimension) and j is such that $\Sigma_{k=1}^{j}\lambda_k>0$ and $\Sigma_{k=1}^{j+1}\lambda_k<0$. D_L is a quite good numerical estimate of the fractal dimension of the attractor.

From the Lyapunov exponent values quoted above, a noninteger Lyapunov dimension $D_L=5.62\pm0.36$ $(j=5)$ is obtained, showing that the attractor has high dimensional fractal qualities.

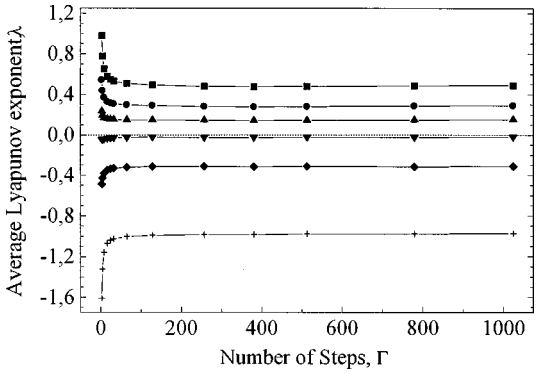

FIG. 11. Lyapunov exponent trends as a function of the number of steps. Each point was obtained by averaging over 5000 locations along the attractor. At $\Gamma=1024$ the exponents are $\lambda_1=0.49\pm0.05$, $\lambda_2=0.29\pm0.05$, $\lambda_3=0.15\pm0.04$, $\lambda_4=-0.02\pm0.007$, $\lambda_5=-0.31\pm0.01$, $\lambda_6=-0.97\pm0.03$ in inverse units of $T_S=10^{-4}$ s.

III. CONCLUDING REMARKS

Nonlinear analyses on the ball trajectories in milling devices demonstrate the hyper-chaotic nature of the system dynamics studied here. Indeed, when previous findings are also taken into consideration, both the powder transformation and the mechanical action of the milling tools are characterized by chaotic features. On one hand, the occurrence of intimate random mixing of macroscopically separated substances has been related to the repetition of the elemental deterministic events such as ball milling collisions.[27] On the other hand, mechanical alloying has been represented as a nonequilibrium process taking place in an open system in which the effects of the self organization of dissipative structures have been modeled by resorting to a fractal approach.[28] A time series of sequential collisions experimentally observed in the real course of a MA process was also investigated by Rustici *et al.*[29] The analyses performed gave evidence for the occurrence of chaotic behavior.

As a consequence a pattern emerges from which it is possible to conclude that chaos occurs at different levels of the ball milling techniques.

Different powder loads, affecting the elasticity conditions of the impacts, also affect the fundamental features of the ball motion. Therefore, it may be of interest to throw light on the influence of the powder charge on the chaotic qualities of the milling process. Further work in this direction is in progress.

ACKNOWLEDGMENTS

This work was supported by CNR (PFMSTAII), COFIN-MURST 97 CFSIB, MURST, and the University of Sassari.

[1] J. S. Benjamin, Mater. Sci. Forum **88–90**, 1–18 (1992).
[2] G. C. Koch, in *Mechanical Milling and Alloying*, Materials Science and Technology, edited by R. W. Cahn, P. Haasen, and E. J. Kramer (Volume editor R. W. Kahn) (VCH, Weinheim 1991), Vol. 15, pp. 193–246.
[3] B. B. Khina and F. H. Froes, J. Met. **48–7**, 36–38 (1996).
[4] *Proceedings of the 1997 International Symposium on Mechanical Alloyed, Metastable and Nanocrystalline Materials*, ISMANAM 1997, Sitges (Barcellona), Spain, 31 August–5 September 1997.
[5] G. Mulas, L. Schiffini, and G. Cocco, ''Impact frequency and energy transfer in milling processes: an experimental approach,'' Mater. Sci. Forum **225–227**, 237–242 (1996).
[6] F. Delogu, M. Monagheddu, G. Mulas, L. Schiffini, and G. Cocco, ''Im-

pact characteristics and Mechanical Alloying processes by ball milling. Experimental evaluation and modelling outcames,'' IJNEP **11-3** (1998).
[7] F. C. Moon, *Chaotic and Fractal Dynamics: An Introduction for Applied Scientists and Engineers* (Wiley, New York, 1992).
[8] E. Ott, *Chaos in Dynamical Systems* (Cambridge University Press, New York, 1993).
[9] J. P. Ekmann and D. Ruelle, ''Ergodic theory of chaos and strange attractors,'' Rev. Mod. Phys. **57**, 617 (1985).
[10] H. D. I. Abarbanel, *Analysis of Observed Chaotic Data* (Springer-Verlag, New York, 1996).
[11] H. D. I. Abarbanel, R. Brown, J. J. Sidorowich, and L. Sh. Tsimring, ''The analysis of observed chaotic data in physical systems,'' Rev. Mod. Phys. **65**, 1331–1392 (1993).
[12] E. H. Love, *A Treatise on the Mathematical Theory of Elasticity*, 4th ed. (Dover, New York, 1944), pp. 193–200.
[13] S. P. Timoshenko and J. N. Goodier, *Theory of Elasticity* (McGraw-Hill, New York, 1970), pp. 409–422.
[14] F. Takens, in *Dynamical Systems and Turbulence*, Lecture Notes in Mathematics, edited by D. A. Rand and L. S. Young (Springer-Verlag, Berlin, 1981), Vol. 898, p. 366.
[15] D. S. Broomhead and G. P. King, ''Exctracting qualitative dynamics from experimental data,'' Physica D **20**, 217 (1986).
[16] A. M. Fraser and H. L. Swinney, ''Independent coordinates for strange attractors from mutual information,'' Phys. Rev. A **33**, 1134–1140 (1986).
[17] Tools for Dynamics, CSP for Windows95, Applied Nonlinear Sciences, LLC and Randle, Inc. (http://www.zweb.com/apnonlin/).
[18] M. B. Kennel, R. Brown, and H. D. I. Abarbanel, ''Determining minimum embedding dimension using a geometrical construction,'' Phys. Rev. A **45**, 3403–3411 (1992).
[19] J. M. Greene and J. S. Kim, ''The calculation of Lyapunov spectra,'' Physica D **13**, 261 (1987).
[20] J. P. Ekmann, S. O. Kamphorst, D. Ruelle, and S. Ciliberto, ''Lyapunov exponents from a time series,'' Phys. Rev. A **34**, 4971 (1986).
[21] A. Wolf, J. B. Swift, H. L. Swinney, and J. A. Vastano, ''Determining Lyapunov exponents from a time series,'' Physica D **16**, 285 (1985).
[22] M. Sano and Y. Sawada, ''Measurement of Lyapunov spectrum from a chaotic time series,'' Phys. Rev. Lett. **55**, 1082 (1985).
[23] P. Bryant and R. Brown, ''Lyapunov exponents from observed time series,'' Phys. Rev. Lett. **65**, 1523 (1990).
[24] P. Bryant, R. Brown, and H. D. I. Abarbanel, ''Computing the Lyapunov spectrum of a dynamical system from an observed time series,'' Phys. Rev. A **43**, 2787 (1991).
[25] H. D. I. Abarbanel and M. B. Kennel, ''Local false neighbors and dynamical dimensions from observed chaotic data,'' Phys. Rev. E **47**, 3057–3068 (1993).
[26] J. Kaplan and J. A. York, *Springer Lecture Notes in Mathematics*, 1979, Vol. 730, p. 204.
[27] P. H. Shingu, K. N. Ishihara, and A. Otsuki, ''Mechanical alloying and chaos,'' Mater. Sci. Forum **179–181**, 5–10 (1995).
[28] P. A. Vityaz, A. A. Kolenikov, A. S. Balankin, and V. S. Ivanova, ''Fractal kinetics of mechanical alloying,'' Mater. Sci. Forum **88–90**, 129–132 (1992).
[29] M. Rustici, G. Mulas, and G. Cocco, ''Detecting chaotic attractors in a ball milling process,'' Mater. Sci. Forum **225–227**, 243–248 (1996).